Mycobacterial Serine/Threonine phosphatase PstP is phospho-regulated and localized to mediate control of cell wall metabolism

Farah Shamma[1], **E. Hesper Rego**[2] **and Cara C. Boutte** [1*]

[1]Department of Biology, University of Texas at Arlington, Arlington, Texas

[2] Department of Microbial Pathogenesis, Yale University School of Medicine, New Haven, Connecticut

***Corresponding author, cara.boutte@uta.edu**

ABSTRACT

The mycobacterial cell wall is profoundly regulated in response to environmental stresses, and this regulation contributes to antibiotic tolerance. The reversible phosphorylation of different cell wall regulatory proteins is a major mechanism of cell wall regulation. Eleven Serine/Threonine protein kinases (STPKs) phosphorylate many critical cell wall-related proteins in mycobacteria. PstP is the sole serine/ threonine phosphatase, but few proteins have been verified as PstP substrates. PstP is itself phosphorylated but the role of its phosphorylation in regulating its activity has been unclear. In this study we aim to discover novel substrates of PstP in *Mycobacterium tuberculosis* (*Mtb*). We show *in vitro* that PstP dephosphorylates two regulators of peptidoglycan in *Mtb*, FhaA and Wag31. We also show that a phospho-mimetic mutation of T137 on PstP negatively regulates its catalytic activity against the cell wall regulators FhaA, Wag31, CwlM, PknB and PknA, and that the corresponding mutation in *Mycobacterium smegmatis (Msmeg)* causes mis-regulation of peptidoglycan *in vivo*. We show that PstP is localized to the septum, which likely restricts its access to certain substrates. These findings on the regulation of PstP provide insight into the control of cell wall metabolism in mycobacteria.

INTRODUCTION

Mycobacterium tuberculosis (*Mtb*), which causes Tuberculosis (TB), remains a public health menace, infecting about 10 million and killing at least a million people worldwide each year (World Health Organization, 2021). TB infections require extended multi-drug antibiotic treatment regimens (Nguyen, 2016). The mycobacterial cell wall contributes to *Mtb*'s inherent antibiotic tolerance (Jarlier and Nikaido, 1994; Sarathy *et al.*, 2013; Batt *et al.*, 2020). The wall serves as permeability barrier (Jarlier and Nikaido, 1990; Hett and Rubin, 2008; Hoffmann *et al.*, 2008; Sarathy *et al.*, 2013), and is strongly regulated in response to stresses (Cunningham and Spreadbury, 1998; Betts *et al.*, 2002; Bhamidi *et al.*, 2012; Sarathy *et al.*, 2013), including infection (Sharma *et al.*, 2006). The cell

40 wall changes in stress are associated with increased antibiotic tolerance (Xie *et*
41 *al.*, 2005; Liu *et al.*, 2016; Sarathy *et al.*, 2017). The expression and activity of
42 many cell wall enzymes and regulators are also tightly coordinated over the
43 course of the cell cycle in order to maintain cell wall integrity during elongation
44 and division (Kieser and Rubin, 2014; Dulberger *et al.*, 2020; Bandekar *et al.*,
45 2020).

46 The cell wall consists of three covalently linked layers: a peptidoglycan layer
47 surrounding the plasma membrane, an arabinogalactan layer and a mycolic acid
48 layer (Marrakchi *et al.*, 2014). Peptidoglycan is a network of glycan chains cross-
49 linked by small peptides, and is the innermost layer of the wall (Abrahams and
50 Besra, 2021). Reversible Serine/Threonine (S/T) phosphorylation of cell wall
51 enzymes and regulators is critical for regulation of cell wall metabolism in
52 response to environmental signals (Wang *et al.*, 1998; Juris *et al.*, 2000;
53 Echenique *et al.*, 2004). There are 11 Serine/Threonine kinases (STPKs) (PknA-
54 B and PknD-L) and one essential S/T protein phosphatase PstP in *Mtb* (Kang *et*
55 *al.*, 2005; Gee *et al.*, 2012; Baer *et al.*, 2014; Boutte *et al.*, 2016)(Cole *et al.*,
56 1998; Bach *et al.*, 2009). PstP is also essential in *Msmeg* (Sharma *et al.*, 2016;
57 DeJesus *et al.*, 2017).

58 PstP belongs to the protein phosphatase 2C (PP2C) subfamily of divalent metal-
59 ion dependent protein serine/threonine phosphatases (Cohen, 1989; Barford,
60 1996; Chopra *et al.*, 2003), which regulate prokaryotic and eukaryotic cell growth
61 and division, sporulation, stress response and metabolic processes in response
62 to various environmental signals (Vijay *et al.*, 2000:2; Irmler and Forchhammer,
63 2001; Mougous *et al.*, 2007; Lu and Wang, 2008; Bradshaw and Losick, 2015;
64 Bradshaw *et al.*, 2017). $PstP_{Mtb}$ shares structural architecture and conserved
65 catalytic residues with the human PP2Cα (Pullen *et al.*, 2004) (Figure 1), the
66 PP2C family prototype. The N-terminal cytoplasmic enzymatic domain of $PstP_{Mtb}$
67 (Figure 1) connects to its C-terminal extracellular domain via a transmembrane
68 helix (Pullen *et al.*, 2004). $PstP_{Mtb}$ is itself phosphorylated on T137, T141, T174
69 and T290 (Figure 1 (Sajid *et al.*, 2011). Phosphorylation on all these sites

70 together affects PstP activity against small molecule substrates *in vitro* (Sajid *et*
71 *al.*, 2011). And phosphorylation on T174 affects cell wall metabolism *in vivo* in
72 *Msmeg* (Shamma *et al.*, 2021).

73 As PstP is the only mycobacterial S/T protein phosphatase (Cole *et al.*, 1998), it
74 likely dephosphorylates many of the substrates phosphorylated by the 11 STPKs
75 (Prisic and Husson, 2014). However, only a few proteins are known PstP
76 substrates: the STPKs PknA and PknB (Boitel *et al.*, 2003; Chopra *et al.*, 2003;
77 Durán *et al.*, 2005; Sajid *et al.*, 2011), mycolic acid biosynthesis enzymes KasA
78 and KasB (Molle *et al.*, 2006), the arabinogalactan regulator EmbR (Sharma *et*
79 *al.*, 2006), and CwlM (Shamma *et al.*, 2021), which in its phosphorylated form is
80 an essential activator of MurA (Boutte *et al.*, 2016), the first enzyme of
81 peptidoglycan precursor synthesis (Marquardt *et al.*, 1992). So
82 dephosphorylation of CwlM~P by PstP (Shamma *et al.*, 2021) should halt
83 peptidoglycan synthesis. CwlM~P also interacts with FhaA (Turapov *et al.*, 2018),
84 which is involved in modulating peptidoglycan biosynthesis (Gee *et al.*, 2012;
85 Viswanathan *et al.*, 2015; Viswanathan *et al.*, 2017) and unphosphorylated CwlM
86 interacts with the peptidoglycan precursor lipid-II flippase MurJ (Turapov *et al.*,
87 2018), suggesting that CwlM may regulate multiple steps in peptidoglycan
88 synthesis (Turapov *et al.*, 2018).

89 FhaA and Wag31 are both regulators of mycobacterial cell wall metabolism.
90 FhaA helps maintain cell envelope integrity, cell length and antibiotic tolerance
91 (Viswanathan *et al.*, 2015; Viswanathan *et al.*, 2017). FhaA stabilizes PbpA
92 (Viswanathan *et al.*, 2017) and binds and may inhibit the MurJ flippase (Gee *et*
93 *al.*, 2012). FhaA is phosphorylated by PknB (Grundner *et al.*, 2005; Prisic *et al.*,
94 2010; Roumestand *et al.*, 2011), though the role of its phosphorylation is not yet
95 clear. Wag31 localizes at the cell poles (Kang *et al.*, 2005), is essential for polar
96 peptidoglycan synthesis (Kang *et al.*, 2008; Jani *et al.*, 2010) and is
97 phosphorylated by the STPK PknA (Kang *et al.*, 2005). Wag31's phosphorylation
98 may also have a role in controlling peptidoglycan metabolism (Jani *et al.*, 2010).

99 It was not known whether FhaA and Wag31 were actively dephosphorylated, or if
100 their phosphorylated forms were removed through protein degradation.

101 In this study we show that $FhaA_{Mtb}$ and $Wag31_{Mtb}$ are substrates of $PstP_{Mtb}$ *in*
102 *vitro*, and that PstP dephosphorylates Wag31 much faster than it does FhaA or
103 CwlM. We show that the T137E phospho-mimetic mutation of $PstP_{Mtb}$ inhibits
104 $PstP_{Mtb}$'s catalytic activity against the substrates CwlM, FhaA, Wag31, PknB and
105 PknA *in vitro*. Furthermore, the corresponding phospho-mimetic mutation in
106 *Msmeg* leads to misregulation of peptidoglycan metabolism. We also find that
107 PstP is enriched at the cell division site, suggesting that its access to substrates
108 might also control its activity. We suggest a model where PstP's activity against
109 assorted substrates is regulated by substrate affinity and protein localization, and
110 further toggled by the phosphorylations on PstP.

111 **RESULTS**

112 **$PstP_{Mtb}$ dephosphorylates $FhaA_{Mtb}$ and $Wag31_{Mtb}$ *in vitro***

113 $FhaA_{Mtb}$ is phosphorylated by $PknB_{Mtb}$ *in vivo* (Prisic *et al.*, 2010) and *in vitro*
114 (Grundner *et al.*, 2005; Roumestand *et al.*, 2011) on T116 (Roumestand *et al.*,
115 2011). $Wag31_{Mtb}$ is phosphorylated at T73 by $PknA_{Mtb}$ (Kang *et al.*, 2005). To
116 determine if $FhaA_{Mtb}$ and $Wag31_{Mtb}$ are substrates of $PstP_{Mtb}$, we purified full-
117 length His-$FhaA_{Mtb}$, His-$Wag31_{Mtb}$ and phosphorylated them by by His-MBP
118 fusions to the kinase domains of $PknA_{Mtb}$ and $PknB_{Mtb}$. We then added the
119 cytosolic domain of $PstP_{Mtb}$ containing the catalytic domain (His-$PstP_cWT_{Mtb}$) and
120 measured changes in phosphorylation. All the proteins in this study were purified
121 first by nickel column and then by size exclusion chromatography, to ensure
122 proper folding. In all the kinase reaction mixtures in this study, the molar
123 concentrations of the substrates were in excess over the ATP [γ-^{32}P], so that
124 there is no leftover ATP [γ-^{32}P] to allow re-phosphorylation once His-$PstP_c$ is
125 added to the reaction mixture for the phosphatase assay. This experimental
126 setup allows us to measure dephosphorylation in the presence of the kinases
127 without re-phosphorylation happening simultaneously.

128 We phosphorylated His-FhaA$_{Mtb}$ with His-MBP-PknB$_{Mtb}$ and ATP [γ-^{32}P]. After
129 addition of His-PstP$_c$WT$_{Mtb}$, at 1/10th the concentration of the His-FhaA$_{Mtb,}$ the
130 phosphorylation on His-FhaA$_{Mtb}$~P decreased by ~80% in 80 minutes (Figure
131 2a,b). Our control assay with no phosphatase shows that the phosphorylation on
132 His-FhaA$_{Mtb}$~P is stable over time in the phosphatase buffer (Figure 2a, b). We
133 then phosphorylated His-Wag31$_{Mtb}$ with His-MBP-PknA$_{Mtb}$ and ATP [γ-^{32}P], and
134 added His-PstP$_c$WT$_{Mtb}$. With 1/100th the amount of PstP compared to Wag31,
135 Wag31$_{Mtb}$ phosphorylation decreased by about ~90% in 2 minutes (Figure 3a,b),
136 only in the presence of His-PstP$_c$WT$_{Mtb}$. These data show that FhaA$_{Mtb}$ and
137 Wag31$_{Mtb}$ are substrates of PstPWT$_{Mtb}$ *in vitro*.

138 Our previous data that demonstrated PstP$_{Mtb}$ dephosphorylates CwlM$_{Mtb}$
139 (Shamma *et al.*, 2021) is reproducible in our *in vitro* assays with ATP [γ-^{32}P] where
140 we observe a 97% decrease in phosphorylation on His-SUMO-CwlM$_{Mtb}$~P 40 minutes
141 after addition of 1/10th the amount of His-PstP$_c$WT$_{Mtb}$ (Figure 4a, b). In all the assays,
142 we see no phosphorylation signals on the WT and phospho-mimetic PstPs on the
143 autoradiograms (Supplementary figure S3). This is likely because PstP can
144 quickly dephosphorylate itself (Sajid *et al.*, 2011) and the purified forms are thus
145 unphosphorylated.

146 Because measuring the rates of dephosphorylation by PstP against different
147 substrates required different PstP concentrations and timing, we calculated the
148 initial linear rate of dephosphorylation per unit concentration of PstP, in order to
149 compare PstP's activity against different substrates. This comparison indicates
150 that His-PstP$_c$WT$_{Mtb}$ dephosphorylates His-Wag31$_{Mtb}$ more than 500 times faster
151 than His-SUMO-CwlM$_{Mtb}$ and about 2500 times faster than His-FhaA$_{Mtb}$ (Figure
152 4c).

153 **Phospho-mimetic mutation at PstPT137$_{Mtb}$ inhibits phosphatase activity**

154 PstP$_{Mtb}$ is phosphorylated on the conserved threonine (T) residues 137, 141 and
155 174 (Figure 1), and when phosphorylated, shows increased activity against small

156 molecule substrates *in vitro* (Sajid *et al.*, 2011). We hypothesized that
157 phosphorylation of the threonine residues of PstP individually might help regulate
158 PstP's activity by either affecting its catalytic activity broadly, or by specifically
159 affecting substrate affinity or activity against specific substrates. To test this, we
160 made phospho-mimetic (T to E) (Cottin *et al.*, 1999) mutants of $PstP_{Mtb}$ at each of
161 the three conserved phosphorylation sites of $PstP_{Mtb}$ in the catalytic domain and
162 purified them (His-$PstP_c$T137E_{Mtb}, His-$PstP_c$T141E_{Mtb} and His-$PstP_c$T174E_{Mtb}).
163 We previously showed that *in vitro* His-$PstP_c$$WT_{Mtb}$ and His-$PstP_c$T174E_{Mtb}
164 dephosphorylate His-SUMO-$CwlM_{Mtb}$ at the same rate (Shamma *et al.*, 2021).
165 We performed separate *in vitro* phosphatase assays with the substrates His-
166 $FhaA_{Mtb}$, His-$Wag31_{Mtb}$ and His-SUMO-$CwlM_{Mtb}$ with the phospho-mimetic
167 versions of PstP. All three substrates exhibit stable phosphorylation with His-
168 $PstP_c$T137E_{Mtb}, indicating that it is inactive *in vitro* against all three substrates
169 (Figures 2,3,4). This suggests that phosphorylation on T137 of PstP may inhibit
170 its activity against multiple substrates.

171 His-MBP-$PknB_{Mtb}$ and His-MBP-$PknA_{Mtb}$, the STPKs used in these assays, are
172 also confirmed substrates of PstP (Sajid *et al.*, 2011). PknA and PknB are
173 activated to phosphorylate their own substrates when they themselves are
174 phosphorylated at their activation loops (Baer *et al.*, 2014). Because we already
175 had these kinases in our phosphatase assays, we were able to measure
176 dephosphorylation of His-MBP-$PknB_{Mtb}$ and His-MBP-$PknA_{Mtb}$ by PstP in the
177 context of a 10-fold and 5-fold excess of His-SUMO-$CwlM_{Mtb}$ or His-$Wag31_{Mtb}$,
178 respectively. We found that His-$PstP_c$T137E_{Mtb} dephosphorylates both His-MBP-
179 $PknB_{Mtb}$ (Figure 5a,b) and His-MBP-$PknA_{Mtb}$ (Figure 5c,d) more slowly than His-
180 $PstP_c$$WT_{Mtb}$ and the other PstP mutants. This shows that His-$PstP_c$T137E_{Mtb} is
181 inhibited against at least five different substrates.

182

183 **Phospho-mimetic mutations at PstPT141$_{Mtb}$ and PstPT174$_{Mtb}$ moderately**
184 **inhibit Wag31's dephosphorylation**

185 His-PstP$_c$T141E$_{Mtb}$ and His-PstP$_c$T174E$_{Mtb}$ dephosphorylate His-FhaA$_{Mtb}$ (Figure
186 2,4c) and His-SUMO-CwlM$_{Mtb}$ (Figure 4) at about the same rate as His-
187 PstP$_c$WT$_{Mtb}$, but dephosphorylate His-Wag31$_{Mtb}$ about half as fast as His-
188 PstP$_c$WT$_{Mtb}$ (Figure 3,4c). These biochemical data support our hypothesis that
189 phosphorylation on PstP may modulate its substrate specificity. Phosphorylation
190 at T141 and T174 appear to inhibit binding or catalysis of Wag31 but not FhaA or
191 CwlM.

192 **A negative charge on T134 of PstP$_{Msmeg}$ regulates peptidoglycan**
193 **metabolism in starvation**

194 Phosphorylation of CwlM allows it to activate the peptidoglycan precursor
195 enzyme MurA, thereby licensing peptidoglycan synthesis (Boutte *et al.*, 2016).
196 Phosphorylation of CwlM also affects its binding to FhaA and the lipid II flippase
197 MurJ (Turapov *et al.*, 2018). CwlM is quickly dephosphorylated in the transition to
198 stasis (Boutte *et al.*, 2016) likely by PstP (Shamma *et al.*, 2021). The function of
199 phosphorylation on FhaA and Wag31 is not yet clear, but available data (Jani *et*
200 *al.*, 2010; Gee *et al.*, 2012; Viswanathan *et al.*, 2016) suggest it could also affect
201 peptidoglycan metabolism. Dephosphorylation of these regulators could be
202 important for downregulation of peptidoglycan metabolism in stasis.

203 As the phospho-mimetic mutation at PstPT137$_{Mtb}$ inhibits PstP's
204 dephosphorylation of three peptidoglycan regulatory proteins *in vitro* (Figure
205 2,3,4), we sought to determine if the corresponding phospho-site on PstP (T134)
206 might affect peptidoglycan metabolism *in vivo* in *Msmeg*. Although this site is not
207 known to be phosphorylated in PstP$_{Msmeg}$ (Iswahyudi *et al.*, 2019; Le *et al.*, 2020),
208 the PstP proteins are 78% identical between *Msmeg* and *Mtb* and most of PstP's
209 substrates are also conserved, so we reasoned that performing experiments with

210 a negative charge at residue T134 on PstP in *Msmeg* will provide a preliminary
211 approximation of what the effect of phosphorylation on this residue might be in
212 *Mtb.* We made *Msmeg* strains with a phospho-mimetic *pstP*T134E$_{Msmeg}$ allele and
213 a phospho-ablative *pstP*T134A$_{Msmeg}$ allele replacing the wild-type *pstP*. We
214 verified the expression of PstPT134E$_{Msmeg}$ and T134A in these strains under
215 normal growth condition (Figure 6h). We found that PstPT134E$_{Msmeg}$ was stable
216 but PstPT134A$_{Msmeg}$ was not, so we did not use the *pstP*T134A$_{Msmeg}$ allele strains
217 for further experiments. We reported previously that the biological replicates of
218 *pstP*T134E$_{Msmeg}$ mutant strains had inconsistent doubling times (Shamma *et al.*,
219 2021) probably due to potential suppressor mutations. We confirmed that the
220 slow growing clones could, after passaging, accumulate suppressor mutations
221 that allowed them to grow as fast as the *pstP*WT$_{Msmeg}$ strain. To characterize the
222 original *pstP*T134E$_{Msmeg}$ strain, we isolated numerous clones from fresh
223 transformations, and measured the doubling times of each before continuing with
224 experiments. We show data only from clones that grew at the slower rate.

225 We stained both log. phase and starved *pstP*T134E$_{Msmeg}$ and WT$_{Msmeg}$ strains
226 using a fluorescent D-amino acid HADA (Kuru *et al.*, 2012) as a reporter of active
227 peptidoglycan metabolism. We saw a slight increase in length (Figure 6b,d and
228 Supplementary Figure S2a,b) and HADA intensity (Figure 6c,d and
229 Supplementary Figure S2a,b) in the *pstP*T134E$_{Msmeg}$ strains in the log. phase
230 compared to the WT$_{Msmeg}$ strains. After starvation, these differences increased
231 (Figure 6b,c,e and Supplementary Figure S2c,d). WT$_{Msmeg}$ strains quickly
232 downregulate peptidoglycan metabolism upon starvation (Boutte *et al.*, 2016), as
233 the decreased HADA staining (Figure 6c,d,e,f,g) shows. The starved
234 *pstP*T134E$_{Msmeg}$ strains show significantly higher HADA signal than the WT$_{Msmeg}$
235 (Figure 6c, top right panels of d,e and Supplementary Figure S2b,d) indicating a
236 defect in downregulating peptidoglycan metabolism. This suggests that the
237 presence of a constant negative charge on phosphosite T134 of PstP$_{Msmeg}$
238 impairs downregulation of peptidoglycan synthesis, likely by inhibiting PstP's
239 dephosphorylation of peptidoglycan regulators (Figure 2,3,4).

240 The mis-regulation of peptidoglycan metabolism (Figure 6c,d,e,f,g and
241 Supplementary Figure S2b,d) may account for the slower growth of the
242 *pstP*T134E$_{Msmeg}$ strains that we see in our data (Figure 6a), though it is likely that
243 other processes beyond peptidoglycan metabolism are also misregulated, as
244 PstP likely has many substrates involved in diverse processes (Molle *et al.*, 2006;
245 Iswahyudi *et al.*, 2019).

246 **PstP localizes at the septum in exponentially growing *Msmeg* cells**

247 We sought to determine if PstP's activity against its diverse substrates could be
248 regulated through protein localization. We made an *Msmeg* strain carrying an
249 additional copy of *pstPWT*$_{Msmeg}$ fused to *mCherry2B*. By time-lapse fluorescence
250 microscopy, we observed that mCherry2B-PstPWT$_{Msmeg}$ appears to be uniformly
251 distributed along the membrane throughout most of the cell cycle, but becomes
252 localized at the septum before cell separation (Figure 7). These data suggest that
253 PstP is also regulated by its access to substrates at different sites in the cell.

254 **Discussion**

255 Our findings indicate that PstP has different basal activity rates against different
256 substrates (Figure 4c), is regulated by its own phosphorylation (Figure 2,3,4,5) to
257 regulate cell wall metabolism (Figure 6), and that it may also be regulated by its
258 localization (Figure 7).

259 We see that PstPWT$_{Mtb}$ dephosphorylates CwlM$_{Mtb}$, FhaA$_{Mtb}$ and Wag31$_{Mtb}$ at
260 different rates *in vitro* (Figure 4c), with Wag31$_{Mtb}$ being the fastest to be
261 dephosphorylated and FhaA the slowest (Figure 4c). We showed that PstP
262 localizes at the septum, or cell division site, in the exponentially growing *Msmeg*
263 cells (Figure 7). Both FhaA and Wag31 localize at the poles and septum (Gee *et*
264 *al.*, 2012; Hannebelle *et al.*, 2020). Our localization data (Figure 7) suggest that
265 co-localization of PstP with these substrates at the septum may cause both
266 Wag31 and FhaA (Figure 2, 3, 4c) to be more highly phosphorylated at the cell
267 poles than at the septum. As PstP dephosphorylates Wag31 so rapidly (Figure 3,

268 4c), we hypothesize that Wag31 is likely to be largely unphosphorylated at the
269 septum, and may only be phosphorylated at the poles.

270 Our data in Figure 2, 3 and 4 show that negative charges at PstPT141$_{Mtb}$ and
271 T174$_{Mtb}$ slow dephosphorylation of Wag31$_{Mtb}$, but not FhaA$_{Mtb}$ and CwlM$_{Mtb}$.
272 Phosphorylation site T141 is on the flap subdomain and T174 is on the β-sheet
273 core (β8) on PstP$_{Mtb}$ (Pullen *et al.*, 2004), but both are facing into the same
274 groove between these domains (Figure 1). T137 is the first residue of the flap
275 subdomain (Pullen *et al.*, 2004), and it faces away from the groove with the other
276 phospho-sites (Figure 1). We propose that the T141/ T174 groove may contribute
277 to toggling specificity of PstP against certain substrates, depending on the
278 phosphorylation status.

279 A previous study showed that PstP$_{cMtb}$, phosphorylated by co-expression with
280 PknA$_{Mtb}$ or PknB$_{Mtb}$, showed higher activity than unphosphorylated PstP against
281 a non-biological small molecule substrate *in vitro*, while PstP$_{c}$T141E$_{Mtb}$ showed
282 the same activity as the wild-type against the small molecule (Sajid *et al.*, 2011).
283 However, the status of phosphorylation of the other individual phospho-sites on
284 PstP$_{Mtb}$ was not examined in that study. Our study, in contrast, sheds light on the
285 effect of individual phospho-sites against biological protein substrates. Our
286 findings (Figure 2,3, and 4) show that the phospho-mimetic PstP$_{c}$T137E$_{Mtb}$ has
287 an inhibitory effect whereas the phospho-mimetic variants PstP$_{c}$T141E$_{Mtb}$ and
288 PstP$_{c}$T174E$_{Mtb}$ play a role in substrate specificity.

289 Our *in vitro* data in Figure 2, 3, 4 and 5 show that PstPT137E$_{Mtb}$ inhibits its
290 activity against CwlM$_{Mtb}$, FhaA$_{Mtb}$ and Wag31$_{Mtb}$, and also against the STPKs
291 PknA and PknB that phosphorylate them, all of which are involved in regulation
292 of peptidoglycan metabolism (Thakur and Chakraborti, 2006; Kang *et al.*, 2008;
293 Jani *et al.*, 2010; Gee *et al.*, 2012; Prisic and Husson, 2014; Boutte *et al.*, 2016;
294 Viswanathan *et al.*, 2016; Viswanathan *et al.*, 2017; Carette *et al.*, 2018; Turapov
295 *et al.*, 2018). The corresponding residue in PstP$_{Msmeg}$ is T134. Although this
296 residue may not be phosphorylated in PstP$_{Msmeg}$ (Iswahyudi *et al.*, 2019; Le *et al.*,

297 2020), we sought to determine if a negative charge at this site would still affect
298 peptidoglycan metabolism in *Msmeg*, as we would expect from the changes in
299 dephosphorylation of the peptidoglycan regulators from *Mtb.* Our *in vivo* data
300 show that the *pstP*T134E$_{Msmeg}$ strains grow more slowly, and have an increase in
301 cell length and HADA staining, especially in starvation (Figure 6). This suggests
302 that dephosphorylation of CwlM, FhaA, Wag31, PknB or PknA, is important in the
303 transition to stasis and that a negative charge at the T134$_{Msmeg}$/T137$_{Mtb}$ site would
304 inhibit the ability of PstP to properly regulate the cell wall through these and other
305 substrates. In this study, we focus on the residues that are phosphorylated in the
306 PstP protein from *Mtb* (Sajid *et al.*, 2011); while the experiments in *Msmeg* do not
307 predict what effects phosphorylation on PstPT137 would have in *Mtb*, they at
308 least indicate that some effect on peptidoglycan metabolism is probable.

309 Other studies have shown that PstP is an important regulator of cell division and
310 cell length (Sharma *et al.*, 2016). Our work shows that PstP localizes to the cell
311 division site, which corroborates its importance in septation (Figure 7). We also
312 show that the PstPT134E$_{Msmeg}$ mutation affects cell length (Figure 6b), which
313 could be mediated by changes in division or elongation.

314 Although our findings are limited to PstP's activity on certain substrates only, they
315 show that the individual phosphosites are important in regulating PstP. *In vitro*,
316 we see that a negative charge on T137 of PstP$_{Mtb}$ inhibits its activity against three
317 PG regulators (Figure 2,3,4), as well as the essential kinases PknB and PknA
318 when they are mixed together (Figure 5). In the cell, the substrates and kinases
319 also co-exist, and PstP may exert its effect directly by dephosphorylating the
320 substrates or indirectly by acting on the kinase (Bhaskara *et al.*, 2019), or both
321 simultaneously. There are likely other mechanisms of cell wall regulation involved
322 in the complex *in vivo* scenario like protein localization or PstP's interaction with
323 other regulatory proteins that may contribute to PstP's regulation as well. We do
324 not know the conditions under which PstP is phosphorylated, or the combinations
325 of PstP's phosphorylations that exist in the cell. So the *in vitro* data only gives us
326 a hint of the deep complexity of the STPK-substrate-PstP network *in vivo*.

327 In this work we show that PstP is regulated by both phosphorylation and
328 localization. This work demonstrates the importance of protein
329 dephosphorylation, not just phosphorylation, in regulating the activity of proteins
330 involved in cell wall metabolism in mycobacteria. Future work that addresses
331 when all of these important phospho-sites are phosphorylated and
332 dephosphorylated will help us to understand how all these protein regulators
333 contribute to coordinating the construction and integrity of the cell wall in
334 changing conditions.

335 MATERIALS AND METHODS

336 Bacterial strains and culture conditions

337 All *Mycobacterium smegmatis* mc^{2}155 ATCC 700084 cultures were grown in 7H9
338 (Becton, Dickinson, Franklin Lakes, NJ) medium containing 0.003 g/liter catalase,
339 5 g/liter bovine serum albumin (BSA), 2 g/liter dextrose, 0.2% glycerol, 0.85
340 g/liter NaCl, and 0.05% Tween 80 and incubated at 37°C until log. phase. 1xPBS
341 supplemented with 0.05% Tween 80 was used for starvation assays. Cultures
342 were plated on LB Lennox agar (Fisher BP1427-2).

343 *E. coli* Top10, XL1-Blue, and Dh5α strains were used for cloning and *E. coli* BL21
344 Codon Plus and BL21(DE3) strains were used for expressing proteins. Antibiotic
345 concentrations for *M. smegmatis* were 25 µg/ml kanamycin and 20 µg/ml zeocin.
346 Antibiotic concentrations for *E. coli* were 50 µg/ml kanamycin, 25 µg/ml zeocin,
347 20 µg/ml chloramphenicol, and 140 µg/ml ampicillin.

348 Cloning and Strain construction

349 N-terminally Histidine (His) tagged cytosolic domains (1-300 amino acids (Gupta
350 *et al.*, 2009)) of *pstP*$_c$T137E$_{Mtb}$ and *pstP*$_c$T141E$_{Mtb}$, and *fhaA*WT$_{Mtb}$ codon-
351 optimized for expression in *E. coli* were ordered from IDT, Inc. and cloned in to
352 pET28a.

353 The *Msmeg* mc^{2}155 strains Δ*pstP*::lox L5::pCT94-p766tetON6-*pstP*T134E$_{Msmeg}$
354 and Δ*pstP*::lox L5::pCT94-p766tetON6-*pstP*WT$_{Msmeg}$ were generated by L5 allele
355 swapping as described previously (Pashley and Parish, 2003; Shamma *et al.*,
356 2021). All vectors and strains are described in supplementary tables 1-3.

357 A vector that expressed mCherry-2B-PstPWT$_{Msmeg}$ was constructed using
358 isothermal assembly and integrated at the tweety phage integration site in
359 *Msmeg*. In brief, *pstP*WT was amplified from *Msmeg* genomic DNA, and
360 subcloned into a plasmid along with *mCherry2B* and the uv15 ribosomal
361 promoter. The resulting vector was transformed into *Msmeg*.

362 **Growth Curve Assay**

363 At least three biological replicates of *pstP*T134E$_{Msmeg}$ and WT allelic variants
364 were grown in 7H9 medium up to the mid-log. phase. The growth curve assays
365 were performed in non-treated non-tissue culture plates using a plate reader
366 (BioTek Synergy neo2 multi mode reader) in 200µl of 7H9 medium at 37°C
367 starting at an Optical Density at 600nm (OD_{600}) of 0.1.

368 The doubling times of each strain were calculated in the non-linear (curve fit)
369 method using an exponential growth equation with the least squares (ordinary) fit
370 in GraphPad Prism (version 7.0d). *P* values were calculated using two-tailed
371 unpaired t-tests.

372 **Protein purification**

373 His-MBP-PknA$_{Mtb}$ was expressed in *E. coli* BL21(DE3) and all other proteins were
374 expressed using *E. coli* BL21 Codon Plus cells. The *Mtb* genes of all studied
375 factors were cloned into expression vectors. His-MBP-PknB$_{Mtb}$, His-SUMO-
376 CwlM$_{Mtb}$, His-PstP$_c$WT$_{Mtb}$ and His-PstP$_c$T174E$_{Mtb}$ were expressed and purified as
377 previously described (Kieser *et al.*, 2015; Shamma *et al.*, 2021). His-
378 PstP$_c$T137E$_{Mtb}$ and His-PstP$_c$T141E$_{Mtb}$ were expressed and purified using the
379 same conditions and buffers used to purify His-PstP$_c$WT$_{Mtb}$ and His-

380 $PstP_cT174E_{Mtb}$ (Shamma *et al.*, 2021). We purified His-$PstP_cWT_{Mtb}$ and its
381 phospho-mimetic variants using nickel affinity chromatography followed by Size
382 Exclusion chromatography to ensure elution of the correctly folded proteins in the
383 eluate. His-$PstP_cWT_{Mtb}$ and all its phospho-mimetic variants are 34.1KDa and all
384 of them eluted at the same column volume when run on the size exclusion resin
385 (GE Healthcare Sephacryl S-200 in HiPrep 26/70 column). The purification
386 chromatograms were analysed with a standard curve made from running protein
387 standards (BIORAD) on the same size exclusion resin. All the $PstP_c$ variants
388 came out at a column volume where proteins weighing ~35KDa elute according
389 to our standard curve. This indicates that all the PstP variants fold like the wild-
390 type.

391 His-$Wag31_{Mtb}$ was induced with 0.5mM IPTG (isopropyl-*β*-D-
392 thiogalactopyranoside) for 6h at 18°C, and purified on Ni-NTA resin (G-
393 Biosciences 786-940) then dialyzed and concentrated. The buffer for His-
394 $Wag31_{Mtb}$ was 50mM Tris pH 8, 350mM NaCl, 1 mM dithiothreitol (DTT), and
395 10% glycerol. Imidazole (10mM and 20mM) was added to the buffers for lysis of
396 the cell pellets and washing the Ni-NTA resin respectively, and 250mM imidazole
397 was added for elution. The lysis buffer was supplemented with 1mM PMSF and
398 0.2% Triton X100.

399 His-MBP-$PknA_{Mtb}$ (1-279 amino acids containing the kinase domain (Baer *et al.*,
400 2014)) was induced with 0.5mM IPTG at 18°C overnight, purified with 5ml Ni-
401 NTA resins (BIO-RAD EconoFit Nuvia IMAC, 12009287), then run over the size
402 exclusion resin (Enrich SEC650, BIO-RAD 780-1650) after dialysis and
403 concentration to get soluble protein. The buffer for purifying His-MBP-$PknA_{Mtb}$
404 was 50mM Tris pH 7.5, 150mM NaCl, 20% glycerol. PMSF (1mM) was added to
405 the buffer while resuspending the cell pellets. Imidazole was used in buffer for
406 application to (20mM) and for elution from Ni-NTA resin (200mM).

407 His-$FhaA_{Mtb}$ was induced with 1mM IPTG at 18°C overnight and purified on Ni-
408 NTA resin (G-Biosciences, 786-940 in 5 ml Bio-Scale Mini Cartridges, BIO-RAD

409 7324661), then dialyzed, concentrated, and run over size exclusion resin (GE
410 Healthcare Sephacryl S-200 in HiPrep 26/70 column). His-FhaA$_{Mtb}$ was purified
411 using the buffers described in (Roumestand *et al.*, 2011).

412 ***In vitro* dephosphorylation assays**

413 His-SUMO-CwlM$_{Mtb}$ at 0.15 µg/µl (2.64 µM) was phosphorylated *in vitro* with His-
414 MBP-PknB$_{Mtb}$ at 0.015 µg/µl for 30 minutes at room temperature with 0.15µCi/µl
415 ATP [γ-^{32}P] (5x10^{-8} µmol) (3000Ci/mmol, 10mCi/ml, PerkinElmer BLU002A250UC)
416 and 2mM $MnCl_2$ in buffer (50mM Tris, pH 7.5, 250mM NaCl, 10% glycerol and
417 1mM DTT). Right after collecting kinase reaction samples, the leftover mixture
418 was split into equal parts in different microcentrifuge tubes to carry on
419 phosphatase assays by adding replicates of His-PstP$_c$WT$_{Mtb}$, His-PstP$_c$T137E$_{Mtb}$,
420 His-PstPcT141E$_{Mtb}$ or His-PstPcT174E$_{Mtb}$ at 0.012 µg/µl to the kinase reaction
421 mixtures containing 0.12 µg/µl of His-SUMO-CwlM$_{Mtb}$ and incubated in
422 phosphatase buffer (50mM Tris pH 7.5, 10mM $MnCl_2$, and 1mM DTT) at room
423 temperature up to 40 minutes. His-FhaA$_{Mtb}$ at 0.15 µg/µl (2.54 µM) was
424 phosphorylated *in vitro* with His-MBP-PknB$_{Mtb}$ at 0.015 µg/µl for 45 minutes at
425 37°C with 0.15µCi/µl ATP [γ-^{32}P] in presence of 5mM $MnCl_2$ in 25mM Tris pH 7.5
426 and 1mM DTT. Right after collecting 0 minute kinase reaction sample, the
427 reaction mixture was then split into equal parts and incubated with either
428 PstP$_c$WT$_{Mtb}$ or different phospho-mimetic variants of it at 0.012 µg/µl up to 80
429 minutes at room temperature in presence of the phosphatase buffer where the
430 concentration of the substrate was 0.12 µg/µl For CwlM and FhaA, the amount of
431 kinase and phosphatases was 1/10th the amount of substrate, by weight.

432 His-Wag31$_{Mtb}$ at 0.15 µg/µl (4.90 µM) was phosphorylated with His-MBP-PknA$_{Mtb}$
433 at 0.03 µg/µl for 2 hours at room temperature in presence of 0.2µCi/µl ATP [γ-^{32}P]
434 (6.67x10^{-8} µM), 10mM $MnCl_2$ and buffer (50mM Tris pH 7.5, 20% glycerol and 150mM
435 NaCl). The amount of PknA was 1/5th the amount of Wag31 substrate, by weight.

436 The kinase reaction mixture was equally split into separate tubes after the 0

437 second kinase reaction sample was taken. His-PstP$_c$WT$_{Mtb}$ or its different
438 phospho-mimetic variants at 0.0013 µg/µl were added to the mixture containing
439 0.13 µg/µl substrate and incubated at room temperature for up to 120 seconds in
440 the phosphatase buffer. The amount of phosphatase was 1/100th the amount of
441 Wag31 substrate in the phosphatase reactions, by weight.

442 Control samples with no kinase and with no phosphatase were performed in all
443 the above-mentioned substrate dephosphorylation assays. All *in vitro*
444 dephosphorylation assays were carried out separately with two individually
445 purified batches of WT and phospho-mimetic mutant of PstP as biological
446 replicates. In all assays, the substrates were in molar excess over the ATP, so
447 that all the ATP will have been consumed before the phosphatase is added, and
448 re-phosphorylation by the kinases should not occur.

449 **Quantification of γ-^{32}P signals**

450 Samples from each *in vitro* biochemical reaction were collected before (0 minute
451 or second) and after addition of each of the phosphatases at several different
452 time points. The samples were run on 12% (Mini-Protean TGX, BIO-RAD,
453 4561046) gels and stained with Coomassie blue solution. After destaining, gels
454 were dried using the GD200 Vacuum Gel Drying system (Hoefer Inc.) and
455 imaged with phosphor screens (Molecular Dynamics) and a scanner (Storm 860,
456 Amersham Biosciences). ImageQuant software (Molecular Dynamics) was used
457 to process the images.

458 The protein bands on the gel and the phospho-signals on the autoradiogram
459 were then quantified with FIJI. The intensities of the substrate protein bands on
460 the Coomassie-stained gel and their corresponding phospho-signals on the
461 autoradiograms at each time point were normalized against the respective
462 protein band and the phospho-signal at 0 minute (His-SUMO-CwlM$_{Mtb}$ and His-
463 FhaA$_{Mtb}$) or 0 second (His-Wag31$_{Mtb}$) before addition of the phosphatase. These
464 relative intensities were used to calculate the intensity of phospho-signal over the

465 amount of substrate for each time point. These values were used to plot the
466 graph. The γ-^{32}P signal intensities of the kinases on autoradiograms at each time
467 point were normalized against the respective phospho-signal on the kinase at 0
468 minute (His-MBP-PknB$_{Mtb}$) or 0 second (His-MBP-PknA$_{Mtb}$) before addition of the
469 phosphatase. These relative γ-^{32}P signal intensity values were then used to plot
470 the graph in GraphPad Prism (version 7.0d). All values were plotted and p-values
471 were calculated using two-tailed, unpaired Student's t-test in GraphPad Prism
472 (version 7.0d).

473 **Cell staining**

474 At least three biological replicates of *pstP*T134E$_{Msmeg}$ and WT$_{Msmeg}$ allelic variants
475 were grown in 7H9 medium up to mid log. phase. Cultures were washed and
476 then starved in 1xPBS with 0.05% Tween 80 (PBST) at $OD_{600=}$ 0.3 for 15
477 minutes. 100µl of starved culture was then treated with 3µl of 10mM fluorescent
478 D-amino acid HADA for 10 minutes. Cells were then pelleted and resuspended in
479 PBST and fixed with 10µl of 16% paraformaldehyde for 10 minutes at room
480 temperature. Cells were then pelleted and resuspended in PBST before imaging
481 on agarose pads.

482 For staining cells in the log. phase, 1µl of 1mM HADA was added to 100µl
483 culture grown up to the mid-log. phase and incubated at 37°C for 15 minutes.
484 Stained cells were then pelleted, washed and fixed as described above.

485 **Static microscopy and image analysis**

486

487 A Nikon Ti-2 widefield epifluorescence microscope with a Photometrics Prime
488 95B camera and a Plan Apo 100x, 1.45 NA objective lens was used to image
489 cells. A 350/50nm excitation filter and a 460/50nm emission filter were used to
490 take the blue fluorescence images for HADA staining. All images were captured
491 using the NIS Elements software and analyzed using FIJI and MicrobeJ (Ducret
492 *et al.*, 2016). Appropriate parameters for length, width and area were set in

493 MicrobeJ to detect cells. All detected dividing (V-snapping) cells in the images
494 were split at the septum so that each daughter cell could be considered as a
495 single cell. No overlapping cells in the images were included in the analysis.
496
497 Length and mean-intensities of HADA signals of at least 330 cells from each of
498 *pstP*T134E$_{Msmeg}$ and *pstP*WT$_{Msmeg}$ (at least 110 cells from each of three biological
499 replicate strains of each genotype) were quantified using MicrobeJ. The values of
500 the mean intensities of 330 cells of each *pstP* allelic mutant and WT are
501 represented in the graphs generated using GraphPad Prism (version 7.0d).
502
503 The medial intensity profiles of HADA signals in cells from different *pstP* allele
504 strains in log. phase and starvation analyzed with MicrobeJ were plotted on the
505 Y-axis over relative positions of cells using the "XStatProfile" plotting feature in
506 MicrobeJ to show the subcellular localization of fluorescent intensities in cells.
507 Demographs of HADA signal intensity across cell lengths in log. phase and
508 starvation were built using the "Demograph" feature of MicrobeJ by plotting the
509 medial intensity profiles of HADA signals.
510
511 **Time-lapse microscopy**
512
513 An inverted Nikon Ti-E microscope was used for the time-lapse imaging. An
514 environmental chamber was maintained at 37°C. Cells were cultivated in an B04
515 microfluidics plate from CellAsic; continuously supplied with fresh medium; and
516 imaged every 15 minutes using a 60x 1.4 N.A. phase contrast objective, with an
517 intermediate magnification of 1.5x. mCherry2B was excited with a SpectraX
518 Illuminator at 561-nm. Fluorescence was detected with a bandpass filter of 595/40
519 and detected with an ORCA Flash Digital sCMOS.

520 Western Blotting

521 To verify expression of PstPWT$_{Msmeg}$, T134A$_{Msmeg}$ and T134E$_{Msmeg}$, cultures were
522 grown in 10ml of 7H9 medium to OD_{600} = 0.8, pelleted and resuspended in

523 500µl PBS with 1mM phenylmethylsulfonyl fluoride (PMSF), and lysed
524 (MiniBeadBeater-16, model 607, Biospec). The supernatants of the cell lysates
525 were run on 12% resolving Tris-glycine gels and then transferred onto
526 polyvinylidene difluoride (PVDF) membranes (GE Healthcare). To detect PstP-
527 strep-tag II, rabbit anti-Strep-tag II antibody (1:1,000, Abcam, ab76949) in Tris-
528 buffered saline supplemented with Tween 20 (TBST) and 0.5% milk and goat
529 anti-rabbit IgG (H1L) horseradish peroxidase (HRP)-conjugated secondary
530 antibody (1:10,000, Thermo Fisher Scientific 31460) in TBST were used.

531

532 **Acknowledgement:**

533 This work was supported by NIH grant R01AI148917 to CCB and R01AI148255
534 to EHR.

535

536

537 **References:**

538 Abrahams, K.A., and Besra, G.S. (2021) Synthesis and recycling of the mycobacterial
539 cell envelope. *Current Opinion in Microbiology* **60**: 58–65.

540 Bach, H., Wong, D., and Av-Gay, Y. (2009) Mycobacterium tuberculosis PtkA is a novel
541 protein tyrosine kinase whose substrate is PtpA. *Biochemical Journal* **420**: 155–162.

542 Baer, C.E., Iavarone, A.T., Alber, T., and Sassetti, C.M. (2014) Biochemical and Spatial
543 Coincidence in the Provisional Ser/Thr Protein Kinase Interaction Network of
544 *Mycobacterium tuberculosis*. *J Biol Chem* **289**: 20422–20433.

545 Bandekar, A.C., Subedi, S., Ioerger, T.R., and Sassetti, C.M. (2020) Cell-Cycle-
546 Associated Expression Patterns Predict Gene Function in Mycobacteria. *Current Biology*
547 **30**: 3961-3971.e6.

548 Barford, D. (1996) Molecular mechanisms of the protein serine/threonine phosphatases.
549 *Trends Biochem Sci* **21**: 407–412.

550 Batt, S.M., Burke, C.E., Moorey, A.R., and Besra, G.S. (2020) Antibiotics and resistance:
551 the two-sided coin of the mycobacterial cell wall. *The Cell Surface* **6**: 100044.

552 Betts, J.C., Lukey, P.T., Robb, L.C., McAdam, R.A., and Duncan, K. (2002) Evaluation
553 of a nutrient starvation model of Mycobacterium tuberculosis persistence by gene and
554 protein expression profiling. *Molecular Microbiology* **43**: 717–731.

555 Bhamidi, S., Shi, L., Chatterjee, D., Belisle, J.T., Crick, D.C., and McNeil, M.R. (2012)
556 A bioanalytical method to determine the cell wall composition of Mycobacterium
557 tuberculosis grown in vivo. *Analytical Biochemistry* **421**: 240–249.

558 Bhaskara, G.B., Wong, M.M., and Verslues, P.E. (2019) The flip side of phospho-
559 signalling: Regulation of protein dephosphorylation and the protein phosphatase 2Cs.
560 *Plant Cell Environ* **42**: 2913–2930.

561 Boitel, B., Ortiz-Lombardía, M., Durán, R., Pompeo, F., Cole, S.T., Cerveñansky, C., and
562 Alzari, P.M. (2003) PknB kinase activity is regulated by phosphorylation in two Thr
563 residues and dephosphorylation by PstP, the cognate phospho-Ser/Thr phosphatase, in
564 Mycobacterium tuberculosis: Mycobacterial serine/threonine kinase and phosphatase.
565 *Molecular Microbiology* **49**: 1493–1508.

566 Boutte, C.C., Baer, C.E., Papavinasasundaram, K., Liu, W., Chase, M.R., Meniche, X., *et*
567 *al.* (2016) A cytoplasmic peptidoglycan amidase homologue controls mycobacterial cell
568 wall synthesis. *eLife* **5**: e14590.

569 Bradshaw, N., Levdikov, V., Zimanyi, C., Gaudet, R., Wilkinson, A., and Losick, R.
570 (2017) A widespread family of serine/threonine protein phosphatases shares a common
571 regulatory switch with proteasomal proteases. *eLife* **6**.

572 Bradshaw, N., and Losick, R. (2015) Asymmetric division triggers cell-specific gene
573 expression through coupled capture and stabilization of a phosphatase. *eLife* **4**: e08145.

574 Carette, X., Platig, J., Young, D.C., Helmel, M., Young, A.T., Wang, Z., *et al.* (2018)
575 Multisystem Analysis of *Mycobacterium tuberculosis* Reveals Kinase-Dependent
576 Remodeling of the Pathogen-Environment Interface. *mBio* **9**
577 http://mbio.asm.org/lookup/doi/10.1128/mBio.02333-17. Accessed February 15, 2019.

578 Chopra, P., Singh, B., Singh, R., Vohra, R., Koul, A., Meena, L.S., *et al.* (2003)
579 Phosphoprotein phosphatase of Mycobacterium tuberculosis dephosphorylates serine-
580 threonine kinases PknA and PknB. *Biochem Biophys Res Commun* **311**: 112–120.

581 Cohen, P. (1989) The structure and regulation of protein phosphatases. *Annu Rev*
582 *Biochem* **58**: 453–508.

583 Cole, S.T., Brosch, R., Parkhill, J., Garnier, T., Churcher, C., Harris, D., *et al.* (1998)
584 Deciphering the biology of Mycobacterium tuberculosis from the complete genome
585 sequence. **396**: 27.

586 Cottin, V., Linden, A.V., and Riches, D.W.H. (1999) Phosphorylation of Tumor Necrosis
587 Factor Receptor CD120a (p55) by p42mapk/erk2 Induces Changes in Its Subcellular
588 Localization. 14.

589 Cunningham, A.F., and Spreadbury, C.L. (1998) Mycobacterial Stationary Phase Induced
590 by Low Oxygen Tension: Cell Wall Thickening and Localization of the 16-Kilodalton ␣-
591 Crystallin Homolog. *J BACTERIOL* **180**: 8.

592 DeJesus, M.A., Gerrick, E.R., Xu, W., Park, S.W., Long, J.E., Boutte, C.C., *et al.* (2017)
593 Comprehensive Essentiality Analysis of the *Mycobacterium tuberculosis* Genome via
594 Saturating Transposon Mutagenesis. *mBio* **8**: e02133-16, /mbio/8/1/e02133-16.atom.

595 Ducret, A., Quardokus, E.M., and Brun, Y.V. (2016) MicrobeJ, a tool for high throughput
596 bacterial cell detection and quantitative analysis. *Nature Microbiology* **1**: 16077.

597 Dulberger, C.L., Rubin, E.J., and Boutte, C.C. (2020) The mycobacterial cell envelope —
598 a moving target. *Nat Rev Microbiol* **18**: 47–59.

599 Durán, R., Villarino, A., Bellinzoni, M., Wehenkel, A., Fernandez, P., Boitel, B., *et al.*
600 (2005) Conserved autophosphorylation pattern in activation loops and juxtamembrane
601 regions of Mycobacterium tuberculosis Ser/Thr protein kinases. *Biochemical and*
602 *Biophysical Research Communications* **333**: 858–867.

603 Echenique, J., Kadioglu, A., Romao, S., Andrew, P.W., and Trombe, M.-C. (2004)
604 Protein Serine/Threonine Kinase StkP Positively Controls Virulence and Competence in
605 *Streptococcus pneumoniae*. *Infect Immun* **72**: 2434–2437.

606 Gee, C.L., Papavinasasundaram, K.G., Blair, S.R., Baer, C.E., Falick, A.M., King, D.S.,
607 *et al.* (2012) A Phosphorylated Pseudokinase Complex Controls Cell Wall Synthesis in
608 Mycobacteria. *Sci Signal* **5**: ra7–ra7.

609 Grundner, C., Gay, L.M., and Alber, T. (2005) *Mycobacterium tuberculosis*
610 serine/threonine kinases PknB, PknD, PknE, and PknF phosphorylate multiple FHA
611 domains. *Protein Sci* **14**: 1918–1921.

612 Gupta, M., Sajid, A., Arora, G., Tandon, V., and Singh, Y. (2009) Forkhead-associated
613 Domain-containing Protein Rv0019c and Polyketide-associated Protein PapA5, from
614 Substrates of Serine/Threonine Protein Kinase PknB to Interacting Proteins of
615 Mycobacterium tuberculosis. *Journal of Biological Chemistry* **284**: 34723–34734.

616 Hannebelle, M.T.M., Ven, J.X.Y., Toniolo, C., Eskandarian, H.A., Vuaridel-Thurre, G.,
617 McKinney, J.D., and Fantner, G.E. (2020) A biphasic growth model for cell pole
618 elongation in mycobacteria. *Nat Commun* **11**: 452.

619 Hett, E.C., and Rubin, E.J. (2008) Bacterial Growth and Cell Division: a Mycobacterial
620 Perspective. *Microbiology and Molecular Biology Reviews* **72**: 126–156.

621 Hoffmann, C., Leis, A., Niederweis, M., Plitzko, J.M., and Engelhardt, H. (2008)
622 Disclosure of the mycobacterial outer membrane: Cryo-electron tomography and vitreous
623 sections reveal the lipid bilayer structure. *Proceedings of the National Academy of*
624 *Sciences* **105**: 3963–3967.

625 Irmler, A., and Forchhammer, K. (2001) A PP2C-type phosphatase dephosphorylates the
626 PII signaling protein in the cyanobacterium Synechocystis PCC 6803. *Proceedings of the*
627 *National Academy of Sciences* **98**: 12978–12983.

628 Iswahyudi, Mukamolova, G.V., Straatman-Iwanowska, A.A., Allcock, N., Ajuh, P.,
629 Turapov, O., and O'Hare, H.M. (2019) Mycobacterial phosphatase PstP regulates global
630 serine threonine phosphorylation and cell division. *Sci Rep* **9**: 8337.

631 Jani, C., Eoh, H., Lee, J., Hamasha, K., Sahana, M., Han, J.-S., *et al.* (2010) Regulation
632 of Polar Peptidoglycan Biosynthesis by Wag31 Phosphorylation in Mycobacteria. *BMC*
633 *Microbiol* **10**: 327.

634 Jarlier, V., and Nikaido, H. (1990) Permeability barrier to hydrophilic solutes in
635 Mycobacterium chelonei. *J Bacteriol* **172**: 1418–1423.

636 Jarlier, V., and Nikaido, H. (1994) Mycobacterial cell wall: Structure and role in natural
637 resistance to antibiotics. *FEMS Microbiology Letters* 11–18.

638 Juris, S.J., Rudolph, A.E., Huddler, D., Orth, K., and Dixon, J.E. (2000) A distinctive role
639 for the Yersinia protein kinase: Actin binding, kinase activation, and cytoskeleton
640 disruption. *Proceedings of the National Academy of Sciences* **97**: 9431–9436.

641 Kang, C.-M., Abbott, D.W., Park, S.T., Dascher, C.C., Cantley, L.C., and Husson, R.N.
642 (2005) The Mycobacterium tuberculosis serine/threonine kinases PknA and PknB:
643 substrate identification and regulation of cell shape. *Genes Dev* **19**: 1692–1704.

644 Kang, C.-M., Nyayapathy, S., Lee, J.-Y., Suh, J.-W., and Husson, R.N. (2008) Wag31, a
645 homologue of the cell division protein DivIVA, regulates growth, morphology and polar
646 cell wall synthesis in mycobacteria. *Microbiology* **154**: 725–735.

647 Kieser, K.J., Baranowski, C., Chao, M.C., Long, J.E., Sassetti, C.M., Waldor, M.K., *et al.*
648 (2015) Peptidoglycan synthesis in Mycobacterium tuberculosis is organized into
649 networks with varying drug susceptibility. *PNAS* **112**: 13087–13092.

650 Kieser, K.J., and Rubin, E.J. (2014) How sisters grow apart: mycobacterial growth and
651 division. *Nature Reviews Microbiology* **12**: 550–562.

652 Kuru, E., Hughes, H.V., Brown, P.J., Hall, E., Tekkam, S., Cava, F., *et al.* (2012) In Situ
653 Probing of Newly Synthesized Peptidoglycan in Live Bacteria with Fluorescent D -
654 Amino Acids. *Angewandte Chemie International Edition* **51**: 12519–12523.

655 Le, N.-H., Locard-Paulet, M., Stella, A., Tomas, N., Molle, V., Burlet-Schiltz, O., *et al.*
656 (2020) The protein kinase PknB negatively regulates biosynthesis and trafficking of
657 mycolic acids in mycobacteria. *J Lipid Res* jlr.RA120000747.

658 Liu, Y., Tan, S., Huang, L., Abramovitch, R.B., Rohde, K.H., Zimmerman, M.D., *et al.*
659 (2016) Immune activation of the host cell induces drug tolerance in *Mycobacterium*
660 *tuberculosis* both in vitro and in vivo. *J Exp Med* **213**: 809–825.

661 Lu, G., and Wang, Y. (2008) FUNCTIONAL DIVERSITY OF MAMMALIAN TYPE
662 2C PROTEIN PHOSPHATASE ISOFORMS: NEW TALES FROM AN OLD FAMILY:
663 Function of PP2C isoforms. *Clinical and Experimental Pharmacology and Physiology*
664 **35**: 107–112.

665 Marquardt, J.L., Siegele, D.A., Kolter, R., and Walsh, C.T. (1992) Cloning and
666 sequencing of Escherichia coli murZ and purification of its product, a UDP-N-
667 acetylglucosamine enolpyruvyl transferase. *J Bacteriol* **174**: 5748–5752.

668 Marrakchi, H., Lanéelle, M.-A., and Daffé, M. (2014) Mycolic Acids: Structures,
669 Biosynthesis, and Beyond. *Chemistry & Biology* **21**: 67–85.

670 Molle, V., Brown, A.K., Besra, G.S., Cozzone, A.J., and Kremer, L. (2006) The
671 Condensing Activities of the Mycobacterium tuberculosis Type II Fatty Acid Synthase
672 Are Differentially Regulated by Phosphorylation. *Journal of Biological Chemistry* **281**:
673 30094–30103.

674 Mougous, J.D., Gifford, C.A., Ramsdell, T.L., and Mekalanos, J.J. (2007) Threonine
675 phosphorylation post-translationally regulates protein secretion in Pseudomonas
676 aeruginosa. *Nat Cell Biol* **9**: 797–803.

677 Nguyen, L. (2016) Antibiotic resistance mechanisms in M. tuberculosis: an update. *Arch*
678 *Toxicol* **90**: 1585–1604.

679 Pashley, C.A., and Parish, T. (2003) Efficient switching of mycobacteriophage L5-based
680 integrating plasmids in *Mycobacterium tuberculosis*. *FEMS Microbiology Letters* **229**:
681 211–215.

682 Prisic, S., Dankwa, S., Schwartz, D., Chou, M.F., Locasale, J.W., Kang, C.-M., *et al.*
683 (2010) Extensive phosphorylation with overlapping specificity by Mycobacterium
684 tuberculosis serine/ threonine protein kinases. *Proceedings of the National Academy of*
685 *Sciences* **107**: 7521–7526.

686 Prisic, S., and Husson, R.N. (2014) Mycobacterium tuberculosis Serine/Threonine
687 Protein Kinases. *Microbiology Spectrum* **2**
688 http://www.asmscience.org/content/journal/microbiolspec/10.1128/microbiolspec.MGM2
689 -0006-2013. Accessed February 6, 2019.

690 Pullen, K.E., Ng, H.-L., Sung, P.-Y., Good, M.C., Smith, S.M., and Alber, T. (2004) An
691 Alternate Conformation and a Third Metal in PstP/Ppp, the M. tuberculosis PP2C-Family
692 Ser/Thr Protein Phosphatase. *Structure* **12**: 1947–1954.

693 Roumestand, C., Leiba, J., Galophe, N., Margeat, E., Padilla, A., Bessin, Y., *et al.* (2011)
694 Structural Insight into the Mycobacterium tuberculosis Rv0020c Protein and Its
695 Interaction with the PknB Kinase. *Structure* **19**: 1525–1534.

696 Sajid, A., Arora, G., Gupta, M., Upadhyay, S., Nandicoori, V.K., and Singh, Y. (2011)
697 Phosphorylation of Mycobacterium tuberculosis Ser/Thr Phosphatase by PknA and PknB.
698 *PLoS ONE* **6**: e17871.

699 Sarathy, J., Dartois, V., Dick, T., and Gengenbacher, M. (2013) Reduced Drug Uptake in
700 Phenotypically Resistant Nutrient-Starved Nonreplicating Mycobacterium tuberculosis.
701 *Antimicrobial Agents and Chemotherapy* **57**: 1648–1653.

702 Sarathy, J.P., Via, L.E., Weiner, D., Blanc, L., Boshoff, H., Eugenin, E.A., *et al.* (2017)
703 Extreme Drug Tolerance of *Mycobacterium tuberculosis* in Caseum. *Antimicrobial*
704 *Agents and Chemotherapy* **62** http://aac.asm.org/lookup/doi/10.1128/AAC.02266-17.
705 Accessed February 6, 2019.

706 Shamma, F., Quintanilla, S., Bandekar, A., Sassetti, C., and Boutte, C. (2021)
707 Phosphorylation on PstP Regulates Cell Wall Metabolism and Antibiotic Tolerance in
708 Mycobacterium smegmatis. *Journal of Bacteriology* **203**: e00563-20.

709 Sharma, A.K., Arora, D., Singh, L.K., Gangwal, A., Sajid, A., Molle, V., *et al.* (2016)
710 Serine/Threonine Protein Phosphatase PstP of *Mycobacterium tuberculosis* Is Necessary
711 for Accurate Cell Division and Survival of Pathogen. *Journal of Biological Chemistry*
712 **291**: 24215–24230.

713 Sharma, K., Gupta, M., Krupa, A., Srinivasan, N., and Singh, Y. (2006) EmbR, a
714 regulatory protein with ATPase activity, is a substrate of multiple serine/threonine
715 kinases and phosphatase in *Mycobacterium tuberculosis*. *FEBS Journal* **273**: 2711–2721.

716 Thakur, M., and Chakraborti, P.K. (2006) GTPase Activity of Mycobacterial FtsZ Is
717 Impaired Due to Its Transphosphorylation by the Eukaryotic-type Ser/Thr Kinase, PknA.
718 *J Biol Chem* **281**: 40107–40113.

719 Turapov, O., Forti, F., Kadhim, B., Ghisotti, D., Sassine, J., Straatman-Iwanowska, A., *et*
720 *al.* (2018) Two Faces of CwlM, an Essential PknB Substrate, in Mycobacterium
721 tuberculosis. *Cell Rep* **25**: 57-67.e5.

722 Vijay, K., Brody, M.S., Fredlund, E., and Price, C.W. (2000) A PP2C phosphatase
723 containing a PAS domain is required to convey signals of energy stress to the sB
724 transcription factor of Bacillus subtilis. *Molecular Microbiology* 9.

725 Viswanathan, G., Joshi, S.V., Sridhar, A., Dutta, S., and Raghunand, T.R. (2015)
726 Identifying novel mycobacterial stress associated genes using a random mutagenesis
727 screen in Mycobacterium smegmatis. *Gene* **574**: 20–27.

728 Viswanathan, G., Yadav, S., Joshi, S.V., and Raghunand, T.R. (2016) Insights into the
729 function of FhaA, a cell-division associated protein in mycobacteria. *FEMS Microbiology*
730 *Letters* fnw294.

731 Viswanathan, G., Yadav, S., and Raghunand, T.R. (2017) Identification of Mycobacterial
732 Genes Involved in Antibiotic Sensitivity: Implications for the Treatment of Tuberculosis

733 with β-Lactam-Containing Regimens. *Antimicrobial Agents and Chemotherapy* **61**
734 http://aac.asm.org/lookup/doi/10.1128/AAC.00425-17. Accessed February 6, 2019.

735 Wang, J., Li, C., Yang, H., Mushegian, A., and Jin, S. (1998) A Novel Serine/Threonine
736 Protein Kinase Homologue of *Pseudomonas aeruginosa* Is Specifically Inducible within
737 the Host Infection Site and Is Required for Full Virulence in Neutropenic Mice. *J*
738 *Bacteriol* **180**: 6764–6768.

739 World Health Organization (2021) *Global tuberculosis report 2021*. World Health
740 Organization, Geneva. https://apps.who.int/iris/handle/10665/346387. Accessed
741 November 14, 2021.

742 Xie, Z., Siddiqi, N., and Rubin, E.J. (2005) Differential Antibiotic Susceptibilities of
743 Starved Mycobacterium tuberculosis Isolates. *Antimicrobial Agents and Chemotherapy*
744 **49**: 4778–4780.

745

746

747 **Figure Legends**
748

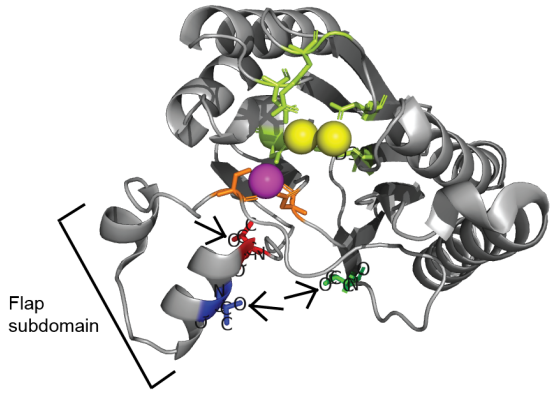

749
750
751 **Figure 1 Phosphorylation sites are not near the active site in PstP**

752 Schematic of the crystal structure of PstP from *M. tuberculosis* ($PstPWT_{Mtb}$) (Pullen
753 *et al.*, 2004) (PDB code 1TXO) showing the conserved threonines (T) which are
754 phosphorylated by the kinases PknA and PknB (Sajid *et al.*, 2011). Highlighted on
755 the structure are: red - T137 (T134 in $PstP_{Msmeg}$); blue - T141 (T138 in $PstP_{Msmeg}$);
756 green - T174 (T171 in $PstP_{Msmeg}$); yellow - Mn^{2+} present at the conserved two-
757 metal center typically seen in the PP2C subfamily of protein Serine/Threonine
758 phosphatases, which are part of the active site core; pink - the unique third Mn^{2+}
759 ion bound in the catalytic core of $PstP_{Mtb}$ but not present in the human PP2Cα
760 which sits in a groove created by the flap subdomain next to the active site; orange
761 - Ser60 and Asp118 that act as ligands for the third Mn ion; lime green - residues
762 of the catalytic sites surrounding the two-metal center. Arrows point to position of
763 the OH-groups on T137, T141 and T174 that are phosphorylated.

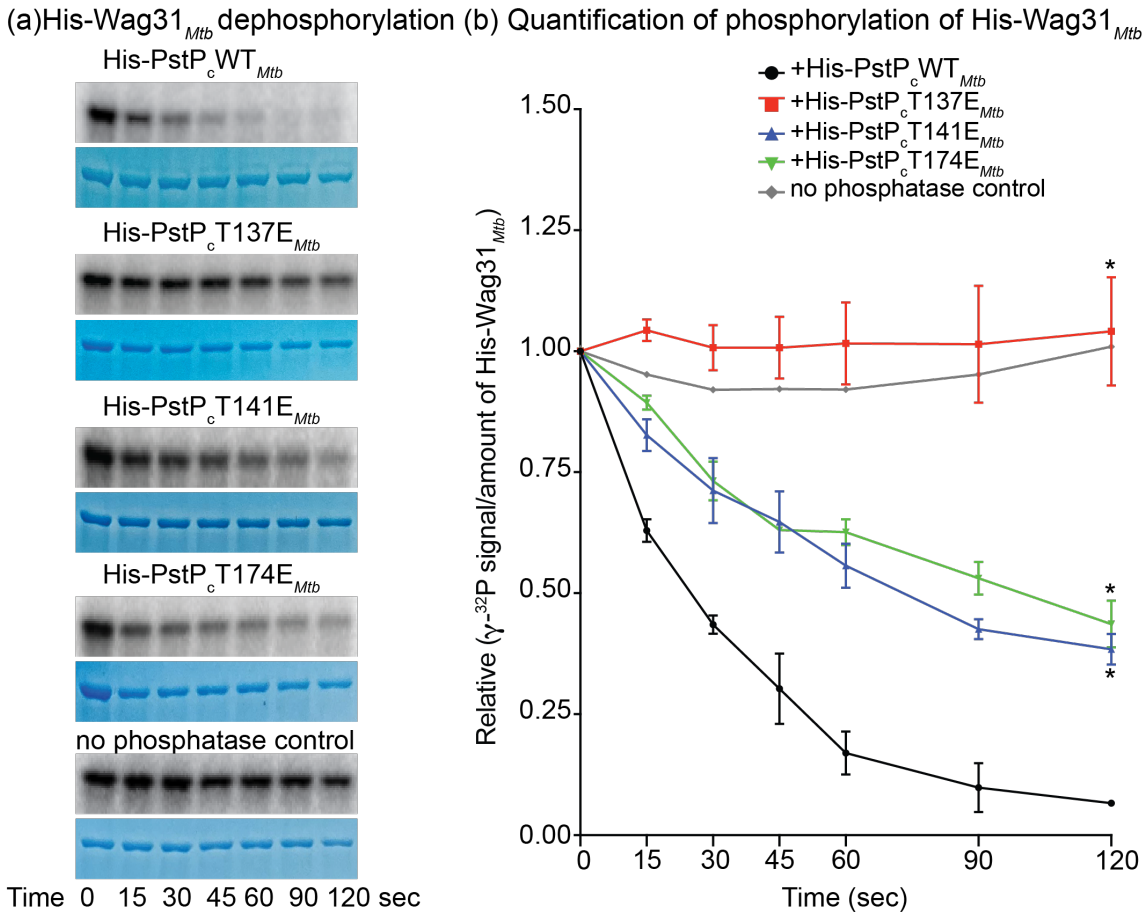

FIGURE 2 Dephosphorylation of FhaA by PstP and phospho-mimetic isoforms.

(a) Autoradiograms and Coomassie-stained SDS gels of *in vitro* phosphatase assays performed with ATP-[γ-^{32}P]-phosphorylated His-FhaA$_{Mtb}$ and His-PstP$_c$WT$_{Mtb}$ (first panel), His-PstP$_c$137E$_{Mtb}$ (second panel), His-PstP$_c$T141E$_{Mtb}$ (third panel), His-PstP$_c$T174E$_{Mtb}$ (fourth panel) and no phosphatase control reaction (bottom panel). The ratio of each phosphatase to His-FhaA$_{Mtb}$ in each of the assays was 1:10. One set of representative images for each assay is shown here from two individual assays performed with individually purified batches of phosphatases.

(b) Quantification of relative intensities of [γ-^{32}P] on His-FhaA$_{Mtb}$ on autoradiogram over the relative amount of His-FhaA$_{Mtb}$ on the SDS gel, average between two replicate experiments. The relative values refer to the normalized values of intensity of [γ-^{32}P] signal and the protein bands on gel at each time point (0 to 80min) with the 0 time point. P values were calculated using two-tailed unpaired t-test.

P-values of T137E at 0 min *vs.* T137E 80 min =0.7598, WT *vs.* T137E at 80 min= 0.0487, WT *vs.* T141E at 80 min =0.3712, WT *vs.* T174E at 80 min=0.2000. The error bars represent standard error of mean.

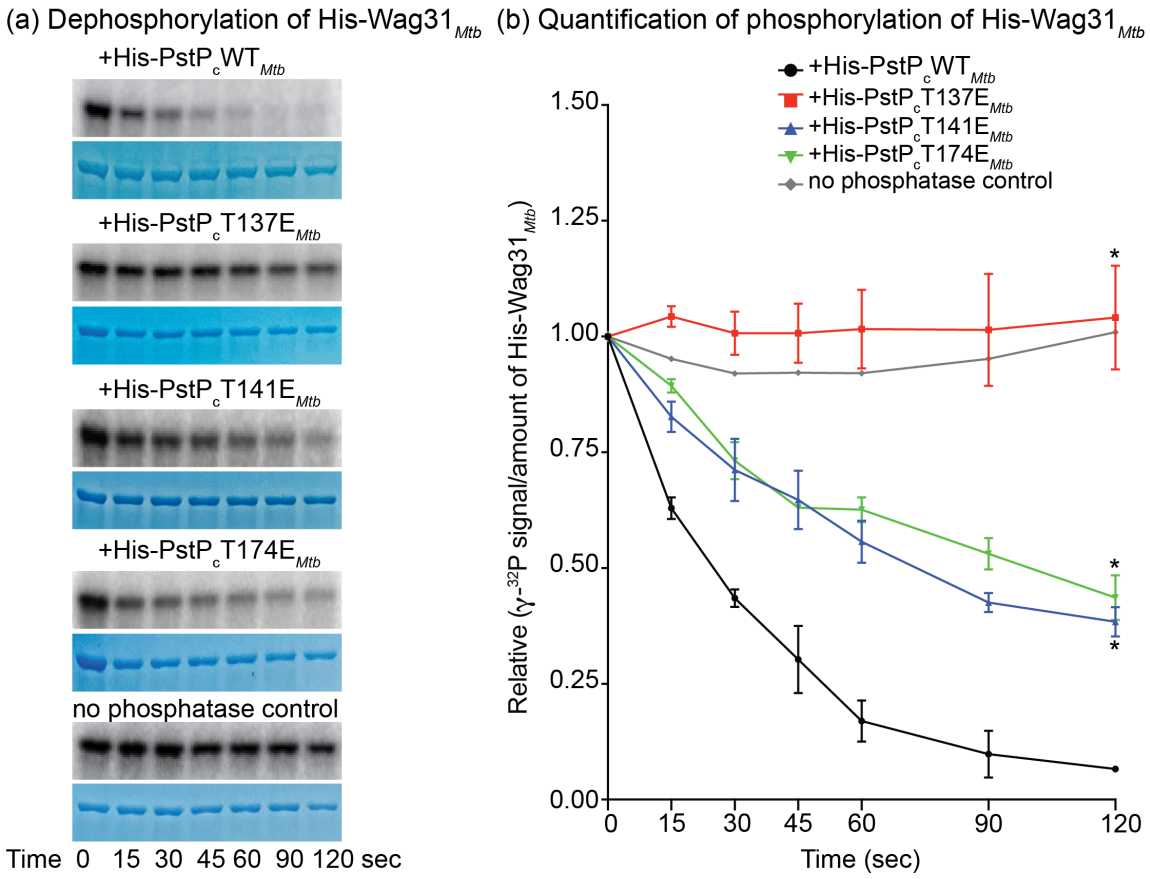

783

784

785

786 **FIGURE 3 Dephosphorylation of Wag31*Mtb* by PstP and phospho-mimetic**
787 **isoforms.**

788

789 (a) Autoradiograms and Coomassie-stained SDS gels of *in vitro* phosphatase
790 assays performed with ATP-[γ-^{32}P]-phosphorylated His-Wag31$_{Mtb}$ and His-
791 PstP$_c$WT$_{Mtb}$ (first panel), His-PstP$_c$WT$_{Mtb}$ (second panel), His-PstP$_c$T141E$_{Mtb}$ (third
792 panel), His-PstP$_c$T174E$_{Mtb}$ (fourth panel) and no phosphatase control reaction
793 (bottom panel). The ratio of each phosphatase to His-Wag31$_{Mtb}$ in the assays was
794 1:100. One set of representative images for each reaction is shown here from two
795 individual assays performed with individually purified batches of phosphatases.

796 (b) Quantification of relative intensities of [γ-^{32}P] on His-Wag31$_{Mtb}$ on
797 autoradiograms over the relative amount of His-Wag31$_{Mtb}$ on the SDS gel, average
798 between two replicate experiments. The relative values are the normalized values
799 of intensity of [γ-^{32}P] signal and the protein bands on gel at each time point (0 to
800 120 sec) with the 0 time point. P values were calculated using two-tailed unpaired
801 t-test.

802 P-values of T137E at 0 sec *vs.* 15 sec = 0. 0.1947 and 0 sec *vs.* 120sec= 0.7493,
803 WT *vs.* T137E at 120 sec= 0.0130, WT *vs.* T141E at 120 sec =0.0106 and WT *vs.*
804 T174E at 120 sec = 0.170. The error bars represent standard error of mean.

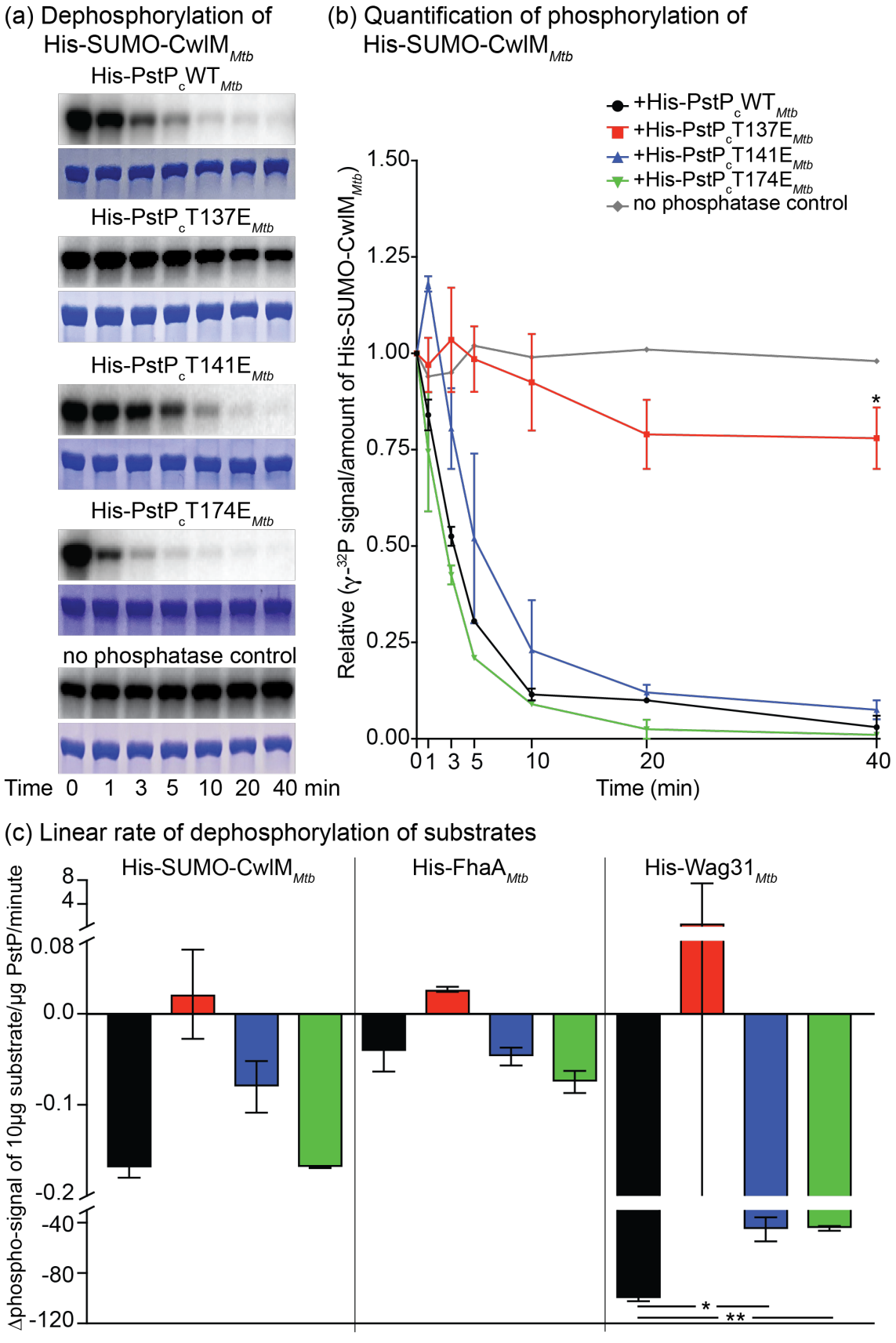
(a) Dephosphorylation of His-SUMO-CwlM$_{Mtb}$
His-PstP$_c$WT$_{Mtb}$
His-PstP$_c$T137E$_{Mtb}$
His-PstP$_c$T141E$_{Mtb}$
His-PstP$_c$T174E$_{Mtb}$
no phosphatase control
Time 0 1 3 5 10 20 40 min
(b) Quantification of phosphorylation of His-SUMO-CwlM$_{Mtb}$
+His-PstP$_c$WT$_{Mtb}$
+His-PstP$_c$T137E$_{Mtb}$
+His-PstP$_c$T141E$_{Mtb}$
+His-PstP$_c$T174E$_{Mtb}$
no phosphatase control
Relative (γ-^{32}P signal/amount of His-SUMO-CwlM$_{Mtb}$)
1.50
1.25
1.00
0.75
0.50
0.25
0.00
0 1 3 5 10 20 40
Time (min)
*
(c) Linear rate of dephosphorylation of substrates
His-SUMO-CwlM$_{Mtb}$
His-FhaA$_{Mtb}$
His-Wag31$_{Mtb}$
Δphospho-signal of 10μg substrate/μg PstP/minute
8
4
0.08
0.0
-0.1
-0.2
-40
-80
-120
*
**

805

806
807 **FIGURE 4 Dephosphorylation of CwlM$_{Mtb}$ by PstP$_{Mtb}$ its phospho-mimetic**
808 **isoforms and linear rate of dephosphorylation of CwlM$_{Mtb}$, FhaA$_{Mtb}$ and**
809 **Wag31$_{Mtb}$**

810 (a) Autoradiograms and Coomassie-stained SDS gels of *in vitro* phosphatase
811 assays performed with ATP-[γ-^{32}P]-phosphorylated His-SUMO-CwlM$_{Mtb}$ and His-
812 PstP$_c$WT$_{Mtb}$ (first panel), His-PstP$_c$WT$_{Mtb}$ (second panel), His-PstP$_c$T141E$_{Mtb}$ (third
813 panel), His-PstP$_c$T174E$_{Mtb}$ (fourth panel) and no phosphatase control reaction
814 (bottom panel). The ratio of each phosphatase to His-SUMO-CwlM$_{Mtb}$ was 1:10.
815 One set of representative images for each reaction is shown here from two
816 individual assays performed with individually purified batches of phosphatases.

817 (b) Quantification of relative intensities of [γ-^{32}P] on His-SUMO-CwlM$_{Mtb}$ on
818 autoradiogram over the relative amount of His-SUMO-CwlM$_{Mtb}$ on the SDS gel,
819 average between two replicate experiments. The relative values are the
820 normalized values of intensity of [γ-^{32}P] signal and the protein bands on gel at each
821 time point (0 to 40min) with the 0 time point. P values were calculated using two-
822 tailed unpaired t-test. P-values of T137E at 0 min *vs.* 40 min= 0.1107, WT *vs*.
823 T137E at 40 min= 0.0127, WT *vs*. T141E at 40 min=0.3683 and WT *vs*. T174E at
824 40 min= 0.5918. The error bars represent standard error of mean.

825 (c) Quantification of linear rate of change in [γ-^{32}P] signal on 10µg of His-SUMO-
826 CwlM$_{Mtb}$, His-FhaA$_{Mtb}$ and His-Wag31$_{Mtb}$ by 1µg His-PstP$_c$WT$_{Mtb}$ and its phospho-
827 mimetic mutants per minute. P values were calculated using two-tailed unpaired t-
828 test. **, *P* value = 0.0026 and *, *P* value 0.0306. The error bars represent standard
829 error of mean.

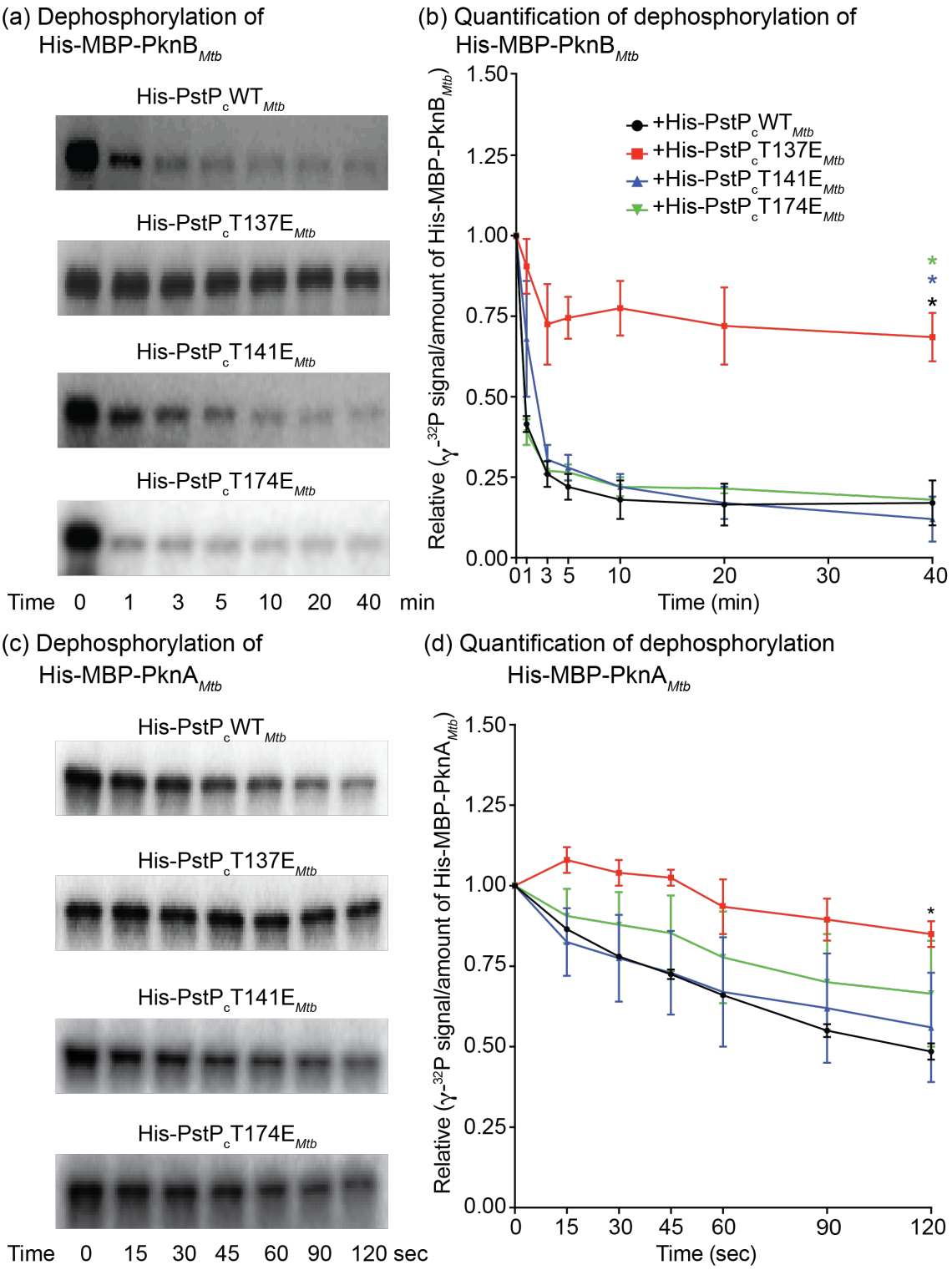

FIGURE 5 Dephosphorylation of PknB$_{Mtb}$ and PknA by PstPWT$_{Mtb}$ and its phospho-mimetic variants

834 (a) Autoradiograms showing [γ-^{32}P]-phospho-signals on His-MBP-PknB$_{Mtb}$ in the *in*
835 *vitro* phosphatase assays with His-SUMO-CwlM$_{Mtb}$ and His-PstP$_c$WT$_{Mtb}$ (first
836 panel), His-PstP$_c$WT$_{Mtb}$ (second panel), His-PstP$_c$T141E$_{Mtb}$ (third panel) and His-
837 PstP$_c$T174E$_{Mtb}$ (fourth panel), where His-MBP-PknB$_{Mtb}$ was used to phosphorylate
838 His-SUMO-CwlM$_{Mtb}$. One set of representative images for each reaction is shown
839 here from two individual assays performed with individually purified batches of
840 phosphatases.

841 (b) Quantification of relative intensities of [γ-^{32}P] on His-MBP-PknB$_{Mtb}$ on
842 autoradiogram, average between two replicate experiments. The relative values
843 refer to the normalized values of intensity of [γ-^{32}P] signal at each time point with
844 the 0 time point. P values were calculated using two-tailed unpaired t-test. P value
845 of T137E at 0 min *vs.* 40 min= 0.0523. *, *P* value= 0.0375 (WT *vs*. T137E at 40
846 min); *, *P* value=0.0314 (T141E *vs*.T137E at 40 min); *, *P* value= 0.0217 (T174E
847 *vs*.T137E at 40 min). The error bars represent standard error of mean.

848 (c) Autoradiograms showing [γ-^{32}P]-phospho-signals on His-MBP-PknA$_{Mtb}$ in the *in*
849 *vitro* phosphatase assays with His-Wag31$_{Mtb}$ and His-PstP$_c$WT$_{Mtb}$ (first panel), His-
850 PstP$_c$WT$_{Mtb}$ (second panel), His-PstP$_c$T141E$_{Mtb}$ (third panel) and His-
851 PstP$_c$T174E$_{Mtb}$ (fourth panel), where His-Wag31$_{Mtb}$ was first phosphorylated with
852 His-MBP-PknA$_{Mtb}$. One set of representative images for each reaction is shown
853 here from two individual assays performed with individually purified batches of
854 phosphatases.

855 (d) Quantification of relative intensities of [γ-^{32}P] on His-MBP-PknA$_{Mtb}$ on
856 autoradiogram. P values were calculated using two-tailed unpaired t-test. The
857 relative values refer to the normalized values of intensity of [γ-^{32}P] signal at each
858 time point with the 0 time point. P value of T137E at 0 sec *vs.* 120 sec= 0.0643. *,
859 *P* value= 0.0163 (WT *vs*. T137E at 120 sec). The error bars represent standard
860 error of mean.

861

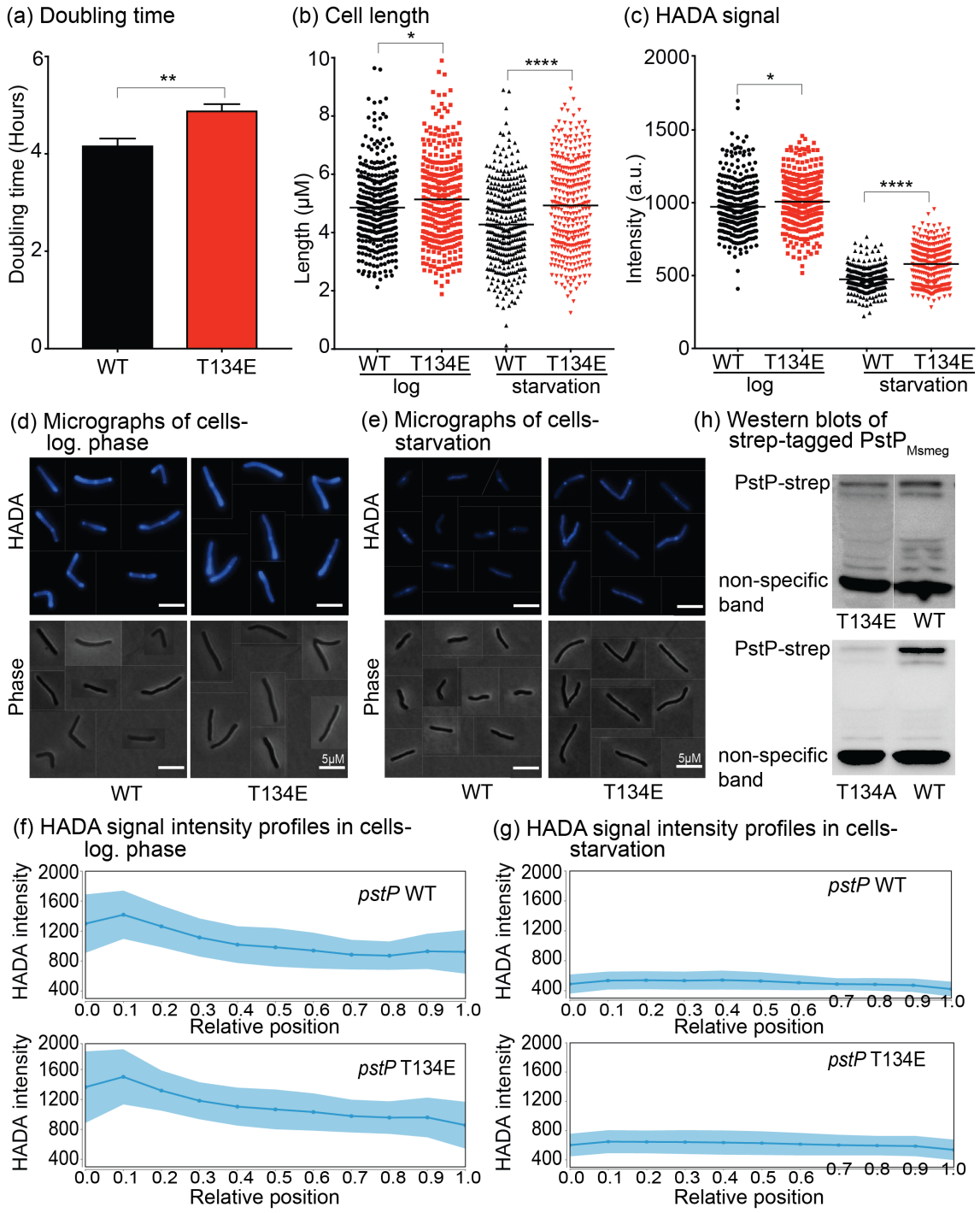

Figure 6 The phosphosite on T134 on PstP$_{Msmeg}$ affects PG metabolism

(a) Doubling times of *Msmeg* strains carrying the *pstP*$_{Msmeg}$ WT and the phosphomimetic T134E (equivalent to T137 on PstP$_{Mtb}$) alleles. Each bar represents the mean of individual average doubling times of three biological replicates of each genotype from two different experiments on different dates. The error bars

870 represent mean with standard deviation. **, *P* value= 0.0026.

871 (b) Quantification of cell lengths of isogenic *pstP*$_{Msmeg}$ allele strains (WT and
872 T134E) grown in 7H9 in log. phase and starved in PBS with Tween80. At least 100
873 cells from each of three biological replicates were quantified. P values were
874 calculated by unpaired t-test. *, *P* value = 0.0122, ****, *P* value= 0.000000031.

875 (c) Quantification of mean intensities of HADA of *pstP*$_{Msmeg}$ allele strains (WT and
876 T134E) grown in 7H9 in log. phase and starved in PBS with Tween80. Cells were
877 stained after 15 minutes of starvation and washed and fixed after another 15
878 minutes (starved for a total of 30 minutes). At least 100 cells from each of three
879 biological replicates were quantified. P values were calculated by unpaired t-test.
880 *, *P* value = 0.0109, ****, *P* value= <0.000000000000001.

881 (d) and (e) Representative HADA and phase images of cells from *pstP*$_{Msmeg}$ allele
882 strains (WT and T134E) grown in 7H9 in log. phase (d) and after 30 minutes of
883 starvation in PBS with Tween80 (e).

884 (f) and (g) Intensity profiles of HADA signals in cells of *pstP*$_{Msmeg}$ allele strains (WT
885 and T134E) in log. phase (f) and after starving for 30 minutes in PBS supplemented
886 with Tween80 (g). The shaded regions denote standard deviations and the solid
887 lines represent the mean intensity values. Signal intensities from at least 110 cells
888 from each of three biological replicates of every *pstP*$_{Msmeg}$ allelic variant genotype
889 were quantified and used to analyze the signal profiles in MicrobeJ. 0 to 1 on the
890 X-axes represent cells from the old pole to the new pole, respectively.

891 (h) α-strep western blots of strep-tagged PstP$_{Msmeg}$ in *pstP*$_{Msmeg}$WT,
892 *pstP*$_{Msmeg}$T134E and *pstP*$_{Msmeg}$T134A allele strains in log. phase. A non-specific
893 band is shown as a loading control.

894

895 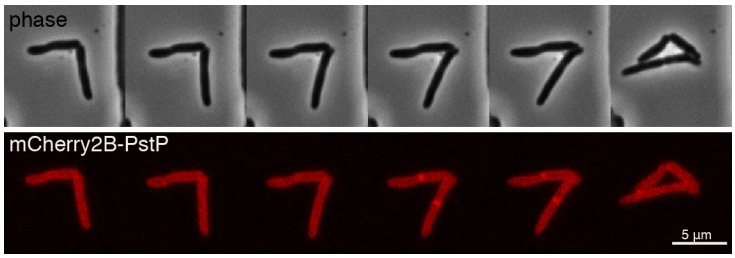

896

897 **Figure 7 PstPWT$_{Msmeg}$ localizes at mid-cell.**

898 *Msmeg* cells expressing mCherry2B-PstPWT$_{Msmeg}$ were imaged over time in a

899 CellAsic Microfluidic device at 15-minute intervals. Intensity is seen at the mid-
900 cell (white arrows) for several frames before cell separation can be visualized by
901 phase contrast microscopy (yellow arrows).

902